Materials Transactions, Vol. 66, No. 8 (2025) pp. 998 to 1005

Mechanical Properties of Powder Metallurgy Extruded Al Based Composites Using Sheath

Mariya Kunichika[1,2], Morimasa Nakamura[1], Takashi Matsuoka[1] and Hidetoshi Somekawa[2,*]

[1]*Department of Mechanical Engineering and Science, Doshisha University, Kyotanabe 610-0394, Japan*
[2]*Research Center for Structural Materials, National Institute for Materials Science, Tsukuba 305-0047, Japan*

The effects of extrusion and dispersed particles (SiC or SiO_2) on the mechanical properties are examined on aluminum (Al) based composites prepared from powder metallurgy. Extrusion is effective for i) grain refinement of the α-Al matrix and ii) producing high quality bulk specimens on a large scale. This is because of a high applied stress during hot-extrusion contributes to the degradation of oxide films covering the powder particles, leading to the creation of new real surfaces. Microstructural observations show that powder-based extruded Al and its composites have fine-grained structures, i.e., an average grain size of less than 5 μm in the α-Al matrix. Accordingly, associated to these microstructures, they show higher strength (∼30 MPa) and hardness (∼10 Hv) than those of cast Al and its composite. In addition to beneficial mechanical properties, the extrusion process does not give a negative impression as for wear property, i.e., the wear rate. Plasticity-controlled void growth mechanism is focused to consider the impact of extrusion on bonding quality. The time required to shrink voids is estimated, and this value is consistent with the actual processing duration. [doi:10.2320/matertrans.MT-M2025050]

(Received April 1, 2025; Accepted May 8, 2025; Published May 30, 2025)

Keywords: *aluminum, extrusion, mechanical property, voids, powder metallurgy*

1. Introduction

Alloying is the most classical and well-known method for improving and controlling the mechanical properties of metallic materials. However, the number of applicable alloying elements is limited, because not all solutes can be dissolved into metallic materials associated with the differences in wettability between solute and solvent atoms. In the case of magnesium (Mg) and aluminum (Al) which are both lightweight metals, there are 29 alloying elements with a maximum solubility of 0.1 at% for Mg and 16 alloying elements for Al [1, 2]. In contrast, based on the powder metallurgy (PM) route, a wide range of particles can be easily dispersed in the base metal matrix, (namely, metal matrix composites); thus, they are recognized as essential materials for structural applications. Metal matrix composites typically exhibit the combined properties of the base metal and dispersed particles, known as the compound law. The added particles also contribute to prevent dislocation slips at room temperature and grain growth at elevated temperatures. As a result, these metal matrix composites have unique and superior properties under a wide range of conditions.

Nevertheless, it is difficult to scale-up the processing for the industrial manufactures and to obtain large-scaled metal matrix composites. Sintering, hot press and hot isostatic press methods are commonly employed to produce these specimens, since the as-received (or raw) material is provided in the powder form. In recent studies, new methods have been reported to resolve these issues. Friction stir processing is effective for uniformly dispersing the added particles with in the matrix and for forming the specimens with higher strength than the base metal [3–6]. Sandwich layer metal matrix composites are pointed out to be fabricated by explosive compaction, potentially providing advantageous mechanical properties [7, 8]. Additive manufacture technique that can be combined with primary processing and final forming is also attracted significant attention [9–11]. In addition to the above-mentioned processes, extrusion that is one of the notable wrought-processes for metallic materials is also utilized to produce metal matrix composites [12–16]. Sintered-specimens and hot pressed-specimens are generally used for the extrusion billet. On the other hands, in such cases, it takes a lot of effort and time to prepare these billets, before extrusion process. In our current studies, the use of sheaths that is made of dissimilar material as compared to the base powder metal is succeeded to produce bulk specimens under a wide range of conditions [17, 18]. Furthermore, this method offers a significant reduction in time and effort, due to simply mixing of powders and then compounding into sheaths.

Based on these knowledges, in this study, Al is selected as the base powder metal, because this metal has a low density and is relatively abundant and affordable. Mg alloy, which is much higher strength and hardness than those of pure Al, is used as the sheath to apply a high magnitude of stress during extrusion. We examined the ability to produce bulk metal matrix composite specimens, comprising SiC or SiO_2 dispersed Al matrix by hot-extrusion. We investigated the mechanical properties of strength and tribology on the Al/SiC and Al/SiO_2 composites, and compared with previously reported Al based composites. Finaly, with focus on void growth mechanism, we considered the role of extrusion on bonding quality and the duration required to shrink the voids. This considered model will give a prediction of suitable condition, i.e., holding time vs. extrusion temperature, and is effective and important from an industrial viewpoint.

2. Experimental Procedures

PM route was applied to produce Al based composites with dispersed SiC or SiO_2 particles having their dispersed fraction, V_f, of 10%. Commercial Al powder with a purity of 99% (≤180 μm in size) and commercial SiC (or SiO_2) powder (∼2 to 3 μm in size) were used in this study. The Al and SiC (or SiO_2) powders were mixed together with Al:SiC

*Corresponding author, E-mail: SOMEKAWA.Hidetoshi@nims.go.jp

(or Al:SiO_2) volume fraction ratio of 9:1 using mortar and pestle. The mixtures were tap-packed by hand pressing into a cylindrical sheath with an inner diameter of 20 mm, inner length of 55 mm, outer diameter of 40 mm and outer length of 70 mm, made of commercial Mg alloy (AZ31). Note that the Mg alloy sheath is beneficial to apply high extrusion load as compared to Al under high temperature. These billets containing the mixed Al and SiC (or SiO_2) powders were kept in a furnace at the temperature of 523 K for more than 30 mins, and then pressed at approximately 1,500 kN for 10 mins. They were subsequently extruded at the ram speed of 0.2 mm/s with an extrusion ratio of 16:1, hereafter denoted as PM-extruded Al/SiC and PM-extruded Al/SiO_2.

To compare specimens with and without SiC (or SiO_2), only the commercial Al powder ($\leq$180 μm in size) was tap-packed into the cylindrical Mg alloy sheath. This billet was extruded under the same conditions as mentioned above, denoted as PM-extruded Al. Apart from these PM extruded specimens, pure Al and Al/SiC composite were produced by casting and they were used for comparison. The cast Al/SiC composite was diluted using Al/SiC with pure Al (99.9%). The dispersed volume fraction, V_f, of SiC was controlled to be 10%, which is the same as that of the PM extruded Al/SiC. It is noted, to the best of our knowledge, that Al/SiC is the only commercial Al based composite that is fabricated by casting process.

Microstructural observations were carried out by electron backscattered diffraction (EBSD) method with accompanying field-emission scanning electron microscopy (FE-SEM) at the scanning step sizes of 2.5 μm or 125 nm. The observed area was the TD-ED planes in the extruded specimens, where TD and ED mean the transverse-direction and extrusion-direction. EBSD data were analyzed using EDAX/TSL software ver. 7.0. Change in the oxide surface covering powder particles attributed to extrusion was examined by transmission electron microscopy (TEM) and X-ray photo-electron spectroscopy (XPS) analysis. For the EBSD observations, their specimens were prepared by polishing to a mirror-like surface finish. TEM specimens were prepared by focused ion beam using the lift-up method.

Mechanical properties were examined by micro-Vickers hardness and compression testing. The magnitude of the applied load was 97 N for a holding time of 15 sec in the hardness test. Each specimen was indented in at least 20 positions. In the compression test, the initial strain rate was 1×10^{-3}/s and the dimension for specimens was a height of 6 mm and a diameter of 3 mm. The compression tests were performed more than three times to confirm the repeatability. In addition to these tests, wear tests were conducted to evaluate the wear rate under the ball-on-disk configuration. The sliding speed was set to 1 mm/s, and counter ball was composed of high-carbon chromium bearing steel (SUJ2) with a diameter of 4.7 mm. The wear rate, K, was calculated using the equation of $K = V/P/L$; P ($= 0.49$ N) is the applied load, L ($= 1{,}000$ mm) is the sliding distance and V is the loss volume. The value of V was measured as the difference in volume before and after wear testing, determined by laser microscopy. Before wear testing, the specimens were polished to a mirror-like surface finish. In specific specimens, the surface features after wear testing were observed by SEM.

3. Results

Cross-sectional features of PM extruded Al before and after extrusion are provided in Fig. 1. Figure 1(a) is the cross-sectional image of the sheath in the just tapped state (i.e., before extrusion). Bright and dark regions indicate Al powder and voids, respectively. This suggests that voids are present before extrusion with an average size of ~100 μm. The inset on the top left-side in Fig. 1(b) is the appearance after extrusion. The length of the produced bulk specimen is more than 300 mm. The contrast at the inner and outer regions are different, indicating the former consists of Al with a diameter of approximately 4 to 5 mm and the latter is Mg associated with the sheath. The cross-sectional image acquired after extrusion shows that there are some traces owning to extrusion with parallel to the process direction, but the voids observed in Fig. 1(a) are found to be clearly extinguished. Inverse pole figure images taken by EBSD are shown in Fig. 2. Figures 2(a) and 2(b) are the micro-structures of the cast pure Al and cast Al/SiC composite. The grain size of the α-Al matrix is coarse; greater than 500 μm for cast Al and ~200 μm for cast Al/SiC, respectively. In Fig. 2(b), SiC particles represented by the black points are dispersed in/around the matrix, which are marked by arrows. Figures 2(c) to 2(e) are the micro-structures of the PM-extruded specimens. Grain structures in

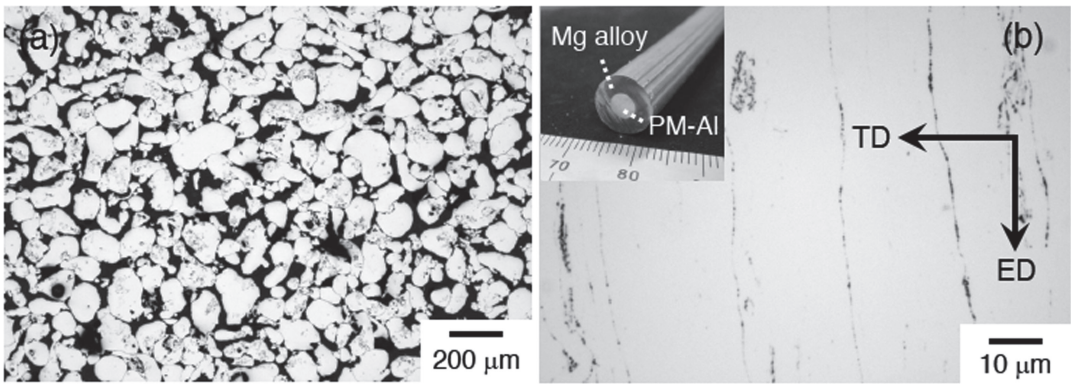

Fig. 1 Cross-sectional images of powder metallurgy extruded Al for (a) before extrusion (just tapped state) and (b) after extrusion. Where top of left-side in Fig. (b) is appearance of bulk specimen, and TD and ED mean the transverse-direction and extrusion-direction.

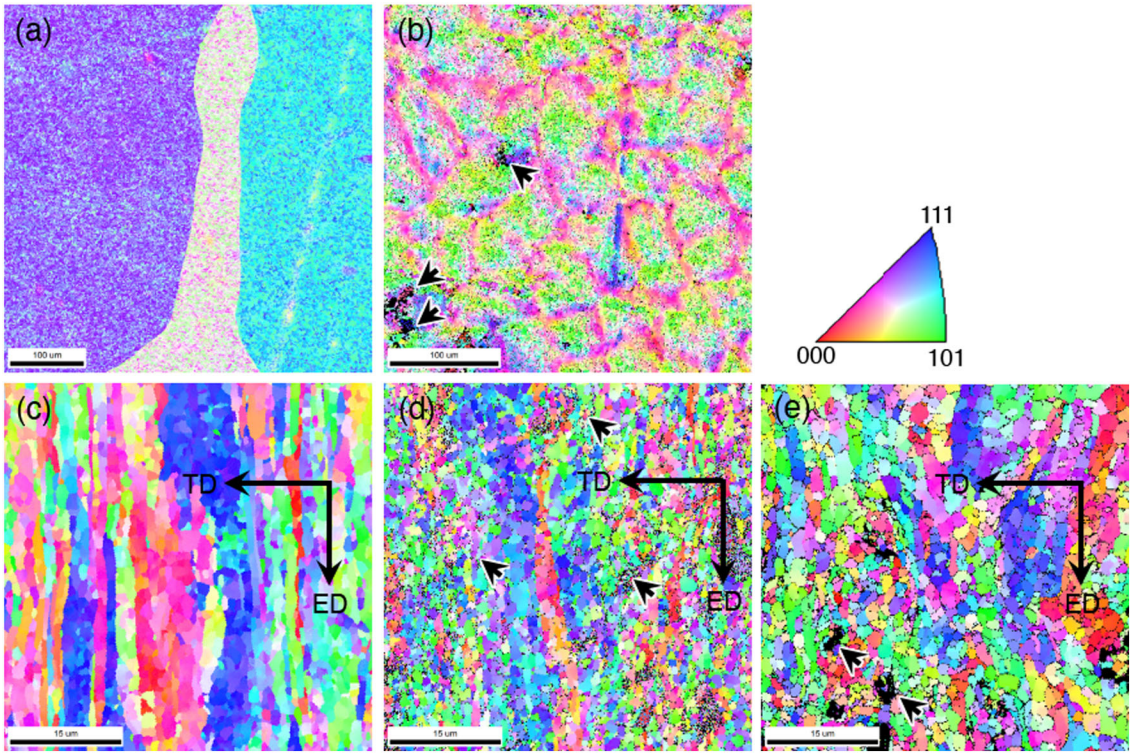

Fig. 2 Inverse pole figure images for (a) cast Al, (b) cast Al/SiC, (c) powder metallurgy extruded Al, (d) powder metallurgy extruded Al/SiC and (e) powder metallurgy extruded Al/SiO_2. Where the black arrows in Figs. (b), (d), (e) indicate dispersed particles, and TD and ED mean the transverse-direction and extrusion-direction. (online color)

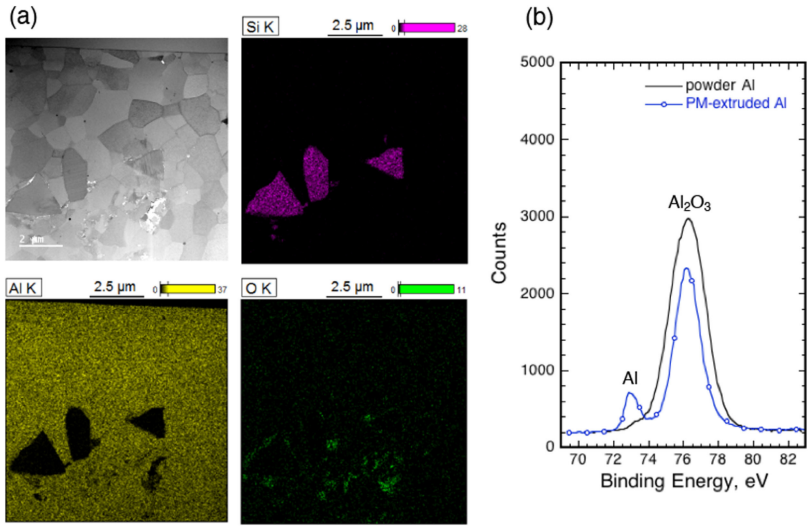

Fig. 3 Change in oxide through extrusion process for (a) TEM observation containing bright field image taken by scanning TEM mode and EDX analysis using powder extruded Al/SiC, (b) XPS analysis for powder pure Al and powder metallurgy extruded Al. (online color)

PM-extruded Al are elongated along the extrusion direction, associated with recovery and recrystallization during hot extrusion. Such a microstructural feature is well-observed in wrought-processed pure Al [19–21]. It is interesting to notice that the grain size of the α-Al matrix is significantly reduced to ∼5 μm in the direction perpendicular to extrusion axis. Similar to PM-extruded Al, the grain size of these composites is ∼2 to 3 μm; while, elongated grain structures are not observed because the dispersed particles are sites for dislocation tangling and recrystallization.

The results obtained from TEM observations of PM-extruded Al/SiC composite are shown in Fig. 3(a). These images include the corresponding compositional maps obtained by energy-dispersive X-ray spectroscopy (EDX). In Fig. 3(a) of top left-side, a bright field image taken by the scanning-TEM mode shows that the observed area contains several SiC particles and voids. EDX mapping shows that oxide presents in void region, as expected. The interfaces between Al and SiC particle contain some oxide, but this is difficult to identify in most interfaces. The XPS analysis for

pure Al before extrusion (powder state in Al) and after extrusion (PM-extruded Al) are provided in Fig. 3(b). In this figure, there is only a strong spectrum for oxide (i.e., Al_2O_3) before extrusion, whereas the extruded Al shows different feature; reduce in oxide spectrum and increase in the Al spectrum. There results appear to show that the extrusion process enhances the atomic scale interfacial bonds between the powders, as a consequence of breaking oxide films.

Nominal stress vs. strain curves in compression are shown in Fig. 4 for (a) cast Al and its composite and (b) PM-extruded Al and its composites. Notably, all compression tests are stopped when the nominal strain reached to 0.4, owing to the measurable limitation of strain gauge. In Fig. 4(b), the inset on the right-side shows the appearance after compression test, which reveals the change to a barrel-shape. Mechanical properties determined from compression and hardness testing are summarized in Table 1. These properties are found to be changed by processing. "PM-extruded" Al and its composites have higher yield strength and hardness than those of "cast" Al and its composite. The Al based composites are also found to exhibit superior yield strength and hardness to those of pure Al, regardless of the processing with or without extrusion. As comparison with PM-extruded specimens, the difference in yield strength (and hardness) between Al and its composite is 25∼55 MPa (and 5∼10 Hv). In general, many factors, such as grain boundary, alloying element (solute), texture and particle dispersion, influence the strength and hardness of materials, which will be considered in later section. However, in simple, considering that they exhibit similar grain sizes in the α-Al matrix, dispersed particles play an important role in strengthening, as a general trend among metal matrix composites.

Surface features after wear testing in PM-extruded specimens are shown in Fig. 5. Figures 5(a) to 5(c) are SEM images, and Figs. 5(d) to 5(f) are three-dimensional profiles taken by laser microscopy. Wear traces are clearly confirmed in all images, and pile-up occurs on both sides of traces. The wear tracks appear to exhibit ductile flow behavior, irrespective of dispersed particle or processing. These results indicate that this wear morphology is classified as typical two-dimensional abrasive wear [22]. Not only the wear testing condition (e.g., lubricant, temperature, magnitude of applied load and sliding speed) but also the mechanical properties of the specimens affect the wear mechanism. Several studies have reported the wear mechanism map, which is a function of external factors (i.e., the load vs. speed) [23–28]. Comparing their maps with the present conditions, abrasive wear is assumed to be the major mechanism, which is consistent with the surface feature as shown in Fig. 5. The wear property (i.e., the specific wear rate) for each specimen is summarized in Table 1 and is provided in Fig. 6. It can be expected that the wear rates in the PM-extruded specimens have relatively high values, because each interface readily becomes a site for delamination. However, similar to the strength, PM-extruded Al and its composites exhibit beneficial wear properties.

4. Discussion

4.1 Effect of extrusion/particle dispersion on mechanical properties

Figures 4 and 6 appear to show that extrusion and particle dispersion are effective in increasing the strength (and hardness) and wear properties. As mentioned above, many factors affect these mechanical properties. Among them, the

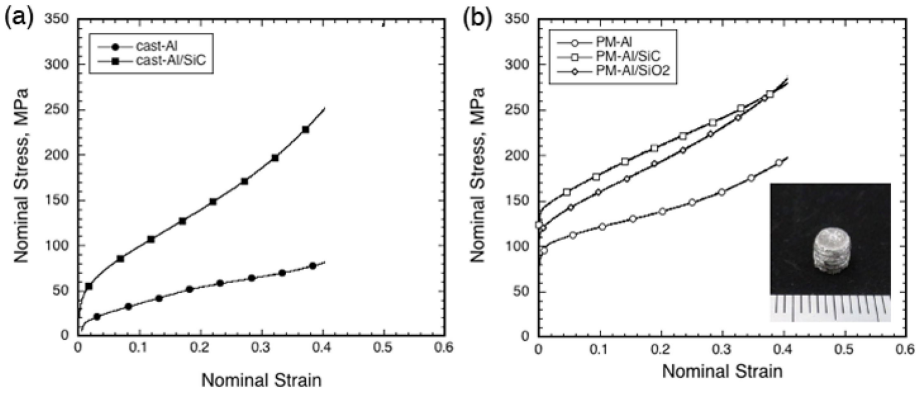

Fig. 4 Nominal stress vs. strain curves in compression for (a) cast specimens and (b) powder metallurgy extruded specimens. Where right side in Fig. (b) is appearance after compression testing. (online color)

Table 1 List of properties obtained from hardness, compression and wear testing.

	H, Hv	σys, MPa	W, $\times 10^{-4}$ mm^3/mN
cast Al	25.2 ± 5.0	15 ± 2	4.77
cast Al/SiC	35.7 ± 6.7	45 ± 2	1.29
PM-extruded Al	41.6 ± 6.3	85 ± 2	4.62
PM-extruded Al/SiC	49.7 ± 7.7	140 ± 3	1.18
PM-extruded Al/SiO_2	44.5 ± 9.9	110 ± 3	1.38

where H is the hardness, σys is the yield strength in compression and W is the wear rate.

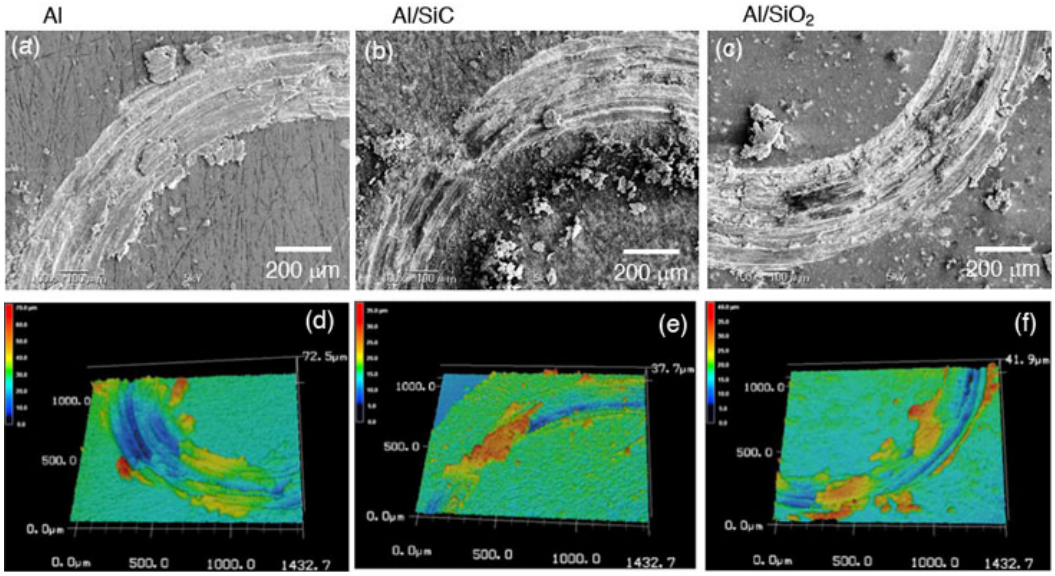

Fig. 5 Surface features after wear testing for (a), (d) powder metallurgy extruded Al, (b), (e) powder metallurgy extruded Al/SiC and (c), (f) powder metallurgy extruded Al/SiO_2. (online color)

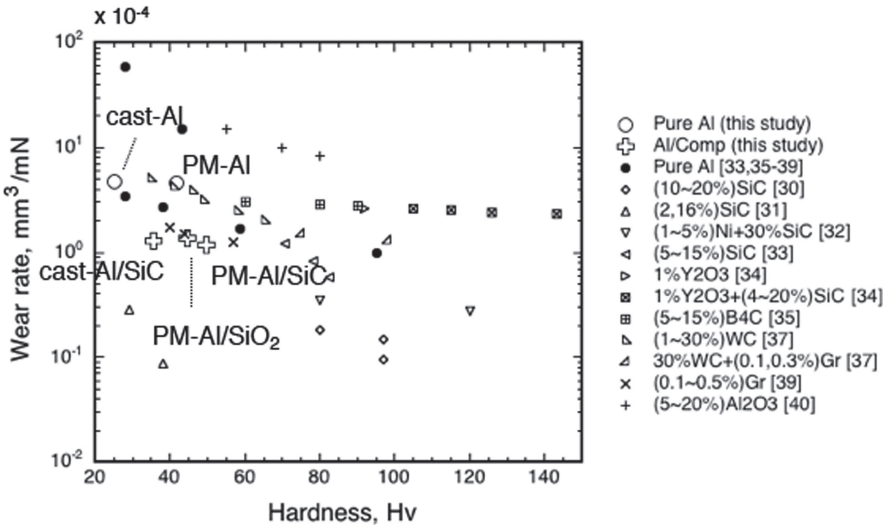

Fig. 6 Relationship between hardness and wear rate of pure Al [33, 35–39] and Al based composites [30–35, 37–40]. Where the values of blank in footnote indicate the fraction of dispersed particles.

most well-known mechanism is grain boundary strengthening, σ_{gb}, which is expressed as follows [41, 42]:

$$\sigma_{gb} = \sigma_0 + k \times d^{-1/2} \quad (1)$$

where σ_0 is the frictional stress, k is the Hall-Petch slope ($= 60\,\mathrm{MPa}\cdot\mu m^2$ in pure Al [43]) and d is the grain size. In Fig. 2, the grain sizes of the cast pure Al and PM-extruded Al are greater than 500 μm and ~5 μm, respectively. By substituting these values for k and d into eq. (1), the contribution of grain boundary strengthening is measured to be approximately 25 MPa ($\approx 25/3.3 = 7.6$ Hv). This estimated values of 25 MPa and 7.6 Hv are lower than the experimental result (70 MPa and 16 Hv in Table 1). Crystal orientation is known to be the other factor that affects strength in wrought-processed metals [44]. In Fig. 2(c), grains are accumulated more along the (111) direction, which suggests that texture strengthening contributes to the enhanced strength in the PM-extruded Al. In addition to these mechanisms, the elongated structure along the wrought-processed direction can bring about increasing strength [45].

Turing to the results of Al composites, these composites have higher strength and hardness than those of pure Al (in Table 1 and Fig. 6). As mentioned above, PM-extruded Al and its composites have similar grained structure, e.g., grain size. The order of them in terms of increasing strength is as follows; the PM-extruded Al < PM-extruded Al/SiO_2 < PM-extruded Al/SiC. The strengthening due to particle dispersion, $\sigma_{particle\text{-}dis}$, is recognized as the Orowan strengthening mechanism, which depends on the factors relating with dispersed particle morphology [46, 47]:

$$\sigma_{particle\text{-}dis} = A \times G \times \varepsilon^{3/2} \times b \times f(V_f \cdot r) \quad (2)$$

where A is a constant, G is the shear modulus, ε is the absolute in misfit strain and b is the Burgers vector. The term of $f(V_f \cdot r)$ is the function of V_f and r, which are the volume fraction and the radius of the dispersed particle, respectively.

Since shear modulus of SiC and SiO_2 are ~130 GPa [48] and 33 GPa [49], this physical factor is simply influential for strength. In the term of misfit strain, this consideration is disregarded here, because of the difficulty in measuring its value in metal matrix composites. In contrast, Fig. 2 reveal that finer particles are dispersed in the PM-extruded Al/SiC as compared to that in the PM-extruded Al/SiO_2, as applicable in eq. (2). The dispersion of reinforced particle, which is a characteristic of high shear modulus and/or consists of fine size, is beneficial for further improvement of the strength and hardness.

Finaly, regarding wear property, the correlation between hardness and wear rate is referred to as the Archard law [29]; a lower wear rate (wear volume) indicates a higher hardness. Figure 6 includes the previous results of pure Al and Al based composites [30–40]. The sliding speed and counter material significantly affect the wear rate. Hardness is also dependent on the type of reinforced particles, as well as their morphology and microstructures of base metal; therefore, these values are somewhat scattered and difficult to compare directly without accounting for these variables. Nevertheless, the dispersion of particles is apparent to have a merit for enhanced hardness and wear properties.

4.2 Estimation of total process duration based on void growth model

Sintering and hot isostatic pressing are the common used methods to fabricate the metal matrix composites from raw powders. In the current study, extrusion was employed to shorten the processing time and to obtain the bulk specimens on a large scale with fewer defects. It hereafter is briefly discussed about the mechanism and role of extrusion, with focusing on the void growth mechanism.

Voids generally grow during plastic flow, particularly in the tensile state. The void growth rate, which is a function of the temperature, strain rate and magnitude of applied stress, is controlled by two famous mechanisms, namely the diffusion-controlled and plasticity-controlled mechanisms [50–53]. They are independent, and the mechanism with the faster growth rate is recognized as the dominant for a given condition. The diffusion-controlled mechanism occurs well at elevated temperatures and low strain rates, whereas the plasticity-controlled mechanism is favorable at high applied stress. Considering the present extrusion condition, the applied stress of ~1,500 kN corresponds to ~1,200 MPa, which is much higher than the room-temperature yield strength (in Fig. 4 and Table 1). In such a case, the plasticity-controlled mechanism is enough to be dominant owing to the small contribution of diffusion. The void growth rate of this mechanism is expressed as follows [52];

$$dr/dt = \dot{\varepsilon} \times \eta/3 \times (r - \gamma/\sigma) \quad (3)$$

where is $\dot{\varepsilon}$ the strain rate, η is the stress factor (= 3 [54]), γ is the surface energy (= 1.2 J/m^2 in Al [54]), r is the void radius and σ is the degree of applied stress. The second term in eq. (3) can be ignored because of the high value for σ. As a result, the void growth rate is roughly re-written as $dr/dt \approx \dot{\varepsilon} \times r$. It is difficult to determine the actual strain rate associated with the two processes (i.e., pressing and extrusion). However, the average strain rate obtained from the total process duration is used and is estimated to be 10^{-3}/s, (where the holding time of 10 mins, the extrusion time of 5 mins and the sheath height of 70 mm). In the case of general extrusion, it is interesting to notice that the strain rate in the present facility is reported to be 10^{-2}/s [55]. As for the void radius of r, this value is assumed to be equivalent to half of the initial void size, ~50 μm (in Fig. 1(a)). Substituting these values of r and $\dot{\varepsilon}$ into eq. (3), the void growth rate is calculated to be approximately 0.05 μm/s. Noted that the direction of applied stress to the billet induces a compressive state during extrusion; that is to say, material flow operates opposite direction. Hence, the growth rate is regarded as a shrinkage rate. For this situation, the void shrinkage size (diameter) by extrusion is estimated to be ~90 μm. Considering that the present used Mg alloy sheath makes it too difficult to perform for wrought-process at room temperature, extrusion must be conducted at elevated temperature ranges (~523 K) in the current case. Such a high temperature is assumed to support powder sintering. Although further studies on the growth/shrinkage mechanism are required, this calculated shrinkage size is similar to the initial void size.

Moreover, the application of high stress during extrusion is effective for producing defect-free bulk specimen. While the oxide film on the surface (in the present case is powder surface) is likely to prevent strong bonding, a new real surface can be created under such severe applied stress levels. For instance, the explosive welding technique has been used for difficult-to-join materials or joining with dissimilar materials [56, 57]. Both the high magnitude of applied stress and high strain rate lead to the removal of the oxide film and to promote bonding quality [58, 59]. Friction welding technique is also another example for the use of high applied stress [60–62]. It is difficult to perform welding/joining in bulk metallic glass, owing to the ease of crystallization through heating effect. A quite high stress, which is much larger than the yield strength in bulk metallic glass, is applied for a very short period. Hence, crystallization is not allowed to occur at the interface, and strength in the bonded specimen does not decrease compared with the initial state. Returning to the current results, herein, Fig. 3 indicates that extrusion causes a change in the oxide films covering the powders particles. A high magnitude of applied stress effectively leads to break oxide films and to create new real surfaces; resulting in enhanced interfacial bonding.

5. Conclusions

In summary, bulk specimens with a long length could be produced from raw powders by extrusion. The results acquired from compression and hardness testing reveal that PM-extruded Al based composites, i.e., Al/SiC and Al/SiO_2, exhibit high strength and hardness while maintaining high compressibility. These extruded Al based composites also have beneficial wear properties without delamination along their particle interfaces. The application of high stress during extrusion plays an important role in degrading the oxide films on the particle and enhancing the bonding quality. Overall, this process is convenient and versatile, enabling the large-scale industrial production of various metal matrix compo-

sites. For instance, from a recycling perspective, waste materials (e.g., metal dust from machining or other industrial by products) can easily be reclaimed and upcycled into valuable products.

Acknowledgements

The authors are grateful to Mr. M. Fukuda (Doshisha University) and Dr. Y. Osawa (National Institute for Materials Science) for their technical help. We are also sincerely thankful for the Japan Fineceramics Co. Ltd., supplied the cast Al/SiC alloy, commercially named as the SA301.

REFERENCES

[1] T.B. Massalski: *Binary Alloy Phase Diagrams*, 2nd ed., (ASM International, Materials Park, OH, 1990).
[2] H. Somekawa: Effect of alloying elements on fracture toughness and ductility in magnesium binary alloys; A review, Mater. Trans. **61** (2021) 1–11.
[3] M. Sharifitabar and H. Nami: Microstructures of dissimilar friction stir welded joints between 2024-T4 aluminum alloy and Al/Mg2Si metal matrix cast composite, Compos. Part B **42** (2011) 2004–2021.
[4] A.K. Srivastava, A. Saxeng and A.R. Dixit: Investigation on the thermal behavior of AZ31B/waste eggshell surface composites produced by friction stir processing, Comp. Comm. **28** (2021) 100912.
[5] A. Sharma, S. Singh and K. Pai: Investigation of microstructural and mechanical properties of Al alloy 7075-T6/B4C nanocomposite concocted via friction stir process, Ceram. Int. **48** (2022) 35708–35718.
[6] N. Bharat and P.S.C. Bose: Microstructure, texture, and mechanical properties analysis of novel AA7178/SiC nanocomposites, Ceram. Int. **49** (2023) 20637–20650.
[7] B. Wang, F. Xie, B. Wang and X. Luo: Microstructure and properties of Ti/Al2O3/NiCr composites fabricated by explosive compaction/cladding, Mater. Sci. Eng. C **50** (2015) 324–331.
[8] S. Vorozhtsov, A. Vorozhtsov, O. Kudryososhova, I. Zhukov and V. Promakhov: Structural and mechanical properties of aluminum-based composites processed by explosive compaction, Pow. Tech. **313** (2017) 251–259.
[9] C. Tan, J. Zou, D. Wang, W. Ma and K. Zhou: Duplex strengthening via SiC addition and in-situ precipitation in additively manufactured composites materials, Compos. Part B **236** (2022) 109820.
[10] C. Shao, C. Lo, K. Bhagavathul, A. McDonald and J. Hogan: High strength particle aluminum matrix composites design: synergistic strengthening strategy, Comp. Comm. **25** (2021) 100697.
[11] C. Liu, K. Jin, J. Ye, X. Gao, X. Wei, Z. Zhang and J. Peng: Additive manufacturing of (TiB+TiC)/Ti6Al4V composites with tailored network reinforcement architecture, Comp. Comm. **40** (2023) 101611.
[12] S. Karabulut, H. Karakoc and R. Citak: Influence of B4C particle reinforcement on mechanical and machining properties of Al6061/B4C composites, Compos. Part B **101** (2016) 87–98.
[13] M. Penchal Reddy, V. Manakari, G. Parande, R.A. Shakoor, A.M.A. Mohamed and M. Gupta: Structural, mechanical and thermal characteristics of Al-Cu-Li particle synthesized by microwave sintering and hot extrusion, Compos. Part B **164** (2019) 485–492.
[14] B. Nateg, M. Haddad-Sabzevar, S.A. Sajjadi, F. Saga, F. Deirming and M. Pellizzari: Architectural design of MWCNT reinforced AlSi10Mg matrix composites with comprehensive mechanical properties, Com. Comm. **25** (2021) 100716.
[15] H. Zhao, T. Yuan, C. Zeng, W. Peng, Z. Sun and H. Hu: Microstructure and mechanical properties of steel wire reinforced Mg matrix composites fabricated by composite extrusion, Com. Comm. **43** (2023) 101711.
[16] H. Watanabe, M. Fukusumi, K. Ishikawa and T. Shimizu: Superplasticity in a fullerene-dispersed Mg-Al-Zn alloy composite, Scr. Mater. **54** (2006) 1575–1580.
[17] H. Somekawa, D. Ando, M. Yamasaki and Y. Kawamura: Microstructure and mechanical properties of low-temperature wrought-processed Mg-Y-Zn alloy containing LPSO phase, Materialia **12** (2020) 100786.
[18] H. Somekawa, M. Yamasaki, Y. Kawamura and T. Inoue: Wrought-procedure memory in caliber rolled Mg-Y-Zn alloy containing LPSO phase, Mater. Charact. **175** (2021) 111080.
[19] Y. Iwahashi, M. Furukawa, Z. Horita, M. Nemoto and T.G. Langdon: Microstructural characteristics of ultrafine-grained aluminum produced using equal-channel angular pressing, Metal. Mater. Trans. A **29** (1998) 2245–2252.
[20] J.P. Hou, R. Li, Q. Wang, H.Y. Yu, Z.J. Zhang, Q.Y. Chen, H. Ma, X.M. Wu, X.W. Li and Z.F. Zhang: Breaking the trade-off relation of strength and electrical conductivity in pure Al wire by controlling texture and grain boundary, J. Alloy. Compd. **769** (2018) 96–109.
[21] B.L. Li, N. Tsuji and N. Kamikawa: Microstructure homogeneity in various metallic materials heavily deformed accumulative roll-bonding, Mater. Sci. Eng. A **423** (2006) 331–342.
[22] T. Yataka, T. Sasaki and S. Kobayashi: Two body abrasive wear of Fe-Al intermetallic compounds, Tetsu-to-Hagané **89** (2003) 1178–1182 (in Japanese).
[23] S.C. Lim: Recent developments in wear-mechanism maps, Tribol. Int. **31** (1998) 87–97.
[24] H. Chen and A.T. Alpas: Sliding wear map for the magnesium alloy Mg-9Al-0.9Zn (AZ91), Wear **246** (2000) 106–116.
[25] C.Y.H. Lim, S.C. Lim and M. Gupta: Wear behavior of SiCp-reinforced magnesium matrix composites, Wear **255** (2003) 629–637.
[26] J. An, R.G. Li, Y. Lu, C.M. Chen, Y. Xu, X. Chen and L.M. Wang: Dry sliding wear behavior of magnesium alloys, Wear **265** (2008) 97–104.
[27] S. Anbu selvan and S. Ramanathan: Dry sliding wear behavior of hot extruded ZK41A magnesium alloy, Mater. Sci. Eng. A **527** (2010) 1815–1820.
[28] A.W. El-Morsy: Dry sliding wear behavior of hot deformed magnesium AZ61 alloy as influenced by the sliding conditions, Mater. Sci. Eng. A **473** (2008) 330–335.
[29] J.F. Archard: Contact and rubbing of flat surfaces, J. Appl. Phys. **24** (1953) 981–988.
[30] Z. Zhang, Z. Wei, Z. Li, B. Hou, R. Xue, H. Xia and Z. Shi: SiC honeycomb reinforced Al matrix composite with improved tribological performance, Ceram. Int. **47** (2021) 23376–23385.
[31] S.M.L. Nai, M. Gupta and C.Y.H. Lim: Synthesis and wear characterization of Al based, free standing functionally graded materials: effects of different matrix composites, Compos. Sci. Technol. **63** (2003) 1895–1909.
[32] C.A. Leon-Patino, E.A. Aguilar-Reyes, E. Bedolla-Becerril, A. Bedolla-Jacuinde and S. Mendez-Diaz: Dry sliding wear of gradient Al-Ni/Si Composites, Wear **301** (2013) 688–694.
[33] F. Jafari, H. Sharifi, M.R. Saeri and M. Tayebi: Effect of refinement volume fraction on the wear behavior of Al-SiCp composites prepared by spark plasma sintering, Sillicon **10** (2018) 2473–2481.
[34] P.P. Shantharaman, V. Anadakrishna, S. Sathish, M. Ravihandran, R. Naveenkumar, S. Jayasathyakawin and S. Rajesh: Investigations on the microstructure and properties of yttria and silicon carbide reinforced aluminum composites, Heliyon **9** (2023) e15462.
[35] Y. Bayrak, A. Kisasoz and R. Sezer: Production and characterization of B_4C content-dependent aluminum matrix composites fabricated via hot pressing, J. Mater. Eng. Perform. **34** (2025) 1607–1618.
[36] B. Venkataraman and G. Sundararajan: The sliding wear behavior of Al-SiC particulate compsoites-1. Macrobehavior, Acta Mater. **44** (1996) 451–460.
[37] A. Taskin and M.C. Senel: Tribological properties and microstructures of tungsten carbide and few-layer graphene-reinforced aluminum based composites, Trans. Indian Inst. Met. **77** (2024) 445–456.
[38] S. Sivakumar, B.R. Golla and K.V. Rajulapati: Influence of ZrB2 hard ceramic reinforcement on mechanical and wear properties of aluminum, Ceram. Int. **45** (2019) 7055–7070.
[39] M.C. Senel, M. Gurbuz and E. Koc: Mechanical and tribological behaviors of aluminum matrix composites reinforced by graphene nanoplatelets, Mater. Sci. Technol. **34** (2018) 1980–1989.
[40] M. Rahimian, N. Parvin and N. Ehsani: Investigation of particle size and amount of alumina on microstructure and mechanical properties of Al matrix composite mad by powder metallurgy, Mater. Sci. Eng. A

527 (2010) 1031–1038.
[41] E.O. Hall: The deformation and aging of mild steel: III discussion of result, Proc. Phys. Soc. B **64** (1951) 747.
[42] N.J. Petch: The cleavage strength of polycrystals, J. Iron Steel Inst. **174** (1953) 25–28.
[43] K. Kubota, M. Mabuchi and K. Higashi: Review Processing and mechanical properties of fine-grained magnesium alloys, J. Mater. Sci. **34** (1999) 2255–2262.
[44] F. Liu, Z.Y. Liu, G.Y. He and L.N. Ou: Dislocation ordering and texture strengthening of naturally aged Al-Cu-Mg alloy, J. Mater. Sci. Technol. **118** (2022) 1–14.
[45] J. Gutierrez-Urrutia, M.A. Munoz-Morris and D.G. Morris: Contribution of microstructural parameters to strengthening in an ultrafine-grained Al-7%Si alloy processed by severe deformation, Acta Mater. **55** (2007) 1319–1330.
[46] A.J. Ardell: Precipitation hardening, Metal. Mater. Trans. A **16** (1985) 2131–2165.
[47] J. Nie: Effects of precipitate shape and orientation on dispersion strengthening in magnesium alloys, Scr. Mater. **48** (2003) 1009–1015.
[48] P.W.M. Peters, E. Martin and P. Pluvinage: Influence of porosity and fibre coating on engineering elastic moduli of fibre-reinforced ceramics (SiC/SiC), Composites **26** (1995) 108–114.
[49] D.J.M. Burkhard: Iron-bearing silicate glasses at ambient conditions, J. Non-Cryst. Solids **275** (2000) 175–188.
[50] W. Beere and M.V. Speight: Creep cavitation by vacancy diffusion in plastically deforming solid, Met. Sci. **12** (1978) 172–176.
[51] R. Raj and M.F. Ashby: Intergranular fracture at elevated temperature, Acta Metall. **23** (1975) 653–666.
[52] A.C.F. Cocks and M.F. Ashby: Intergranular fracture during power-law creep under multiaxial stresses, Met. Sci. **14** (1980) 395–402.
[53] J.W. Hancock: Creep cavitation without a vacancy flux, Met. Sci. **10** (1976) 319–325.
[54] W.R. Tyson and W.A. Miller: Surface free energies of solid metals; Estimation from liquid surface tension measurements, Surf. Sci. **62** (1977) 267–276.
[55] A. Takara, Y. Nishikawa, H. Watanabe, H. Somekawa, T. Mukai and K. Higashi: New forming process of three-dimensionally shaped magnesium parts utilizing high-strain rate superplasticity, Mater. Trans. **45** (2004) 2531–2536.
[56] Y.B. Yan, Z.W. Zhang, W. Shen, J.H. Wang, L.K. Zhang and B.A. Chin: Microstructure and properties of magnesium AZ31B-aluminum 7075 explosively welded composite plate, Mater. Sci. Eng. A **527** (2010) 2241–2245.
[57] D.M. Fronczek, J. Woiewoda-Budka, R. Chulist, A. Sypien, A. Korneva, Z. Szulc, N. Schell and P. Zieba: Structural properties of Ti/Al clads manufactured by explosive welding, Mater. Des. **91** (2016) 80–89.
[58] A.A. Akbari Mousavi and S.T.S. Al-Hassani: Numerical and experimental studies of the mechanism of the wavy interface formations in explosive/impact welding, J. Mechan. Phys. Solids **53** (2005) 2501–2528.
[59] F. Grignon, D. Benson, K.S. Vecchio and M.A. Meyers: Explosive welding of aluminum to aluminum: analysis, computations and experiments, Int. J. Impact Eng. **30** (2004) 1333–1351.
[60] Y. Kawamura and Y. Ohno: Superplastic bonding of bulk metallic glasses using friction, Scr. Mater. **45** (2001) 279–285.
[61] Y. Kawamura and Y. Ohno: Spark welding of Zr55Al10Ni5Cu10 bulk metallic glasses, Scr. Mater. **45** (2001) 127–132.
[62] C.H. Wong and C.H. Shek: Friction welding of Zr41Ti14Cu12.5Be22.5 bulk metallic glass, Scr. Mater. **49** (2003) 393–397.